

RG-Attn: Radian Glue Attention for Multi-modality Multi-agent Cooperative Perception

Lantao Li¹, Kang Yang², Wenqi Zhang¹, Xiaoxue Wang¹ and Chen Sun¹

Abstract—Cooperative perception offers an optimal solution to overcome the perception limitations of single-agent systems by leveraging Vehicle-to-Everything (V2X) communication for data sharing and fusion across multiple agents. However, most existing approaches focus on single-modality data exchange, limiting the potential of both homogeneous and heterogeneous fusion across agents. This overlooks the opportunity to utilize multi-modality data per agent, restricting the system’s performance. In the automotive industry, manufacturers adopt diverse sensor configurations, resulting in heterogeneous combinations of sensor modalities across agents. To harness the potential of every possible data source for optimal performance, we design a robust LiDAR and camera cross-modality fusion module, Radian-Glue-Attention (RG-Attn), applicable to both intra-agent cross-modality fusion and inter-agent cross-modality fusion scenarios, owing to the convenient coordinate conversion by transformation matrix and the unified sampling/inversion mechanism. We also propose two different architectures, named Paint-To-Puzzle (PTP) and Co-Sketching-Co-Coloring (CoS-CoCo), for conducting cooperative perception. PTP aims for maximum precision performance and achieves smaller data packet size by limiting cross-agent fusion to a single instance, but requiring all participants to be equipped with LiDAR. In contrast, CoS-CoCo supports agents with any configuration—LiDAR-only, camera-only, or LiDAR-camera-both, presenting more generalization ability. Our approach achieves state-of-the-art (SOTA) performance on both real and simulated cooperative perception datasets. The code is now available at [GitHub](#).

I. INTRODUCTION

The famous phrase “*United we stand, divided we fall*” by Aesop aptly captures the essence of multi-agent cooperative perception. Shared and fused perception information can be the crucial stepping stone, akin to an oracle’s insight, leading to wiser maneuvering decisions that help prevent traffic accidents as depicted in Fig. 1 (a). By overcoming the limitations of single-agent perception through the exchange of processed sensing data among multiple agents, challenges like non-line-of-sight (NLOS) occluded blind zones, partial object detection and limited detection range can be significantly mitigated. Typically, cooperative perception relies on the integration of V2X wireless communication, sensor data processing, and fusion modules to create a unified collaboration platform. Beyond intelligent traffic systems, cooperative perception can also be applied in multi-robot automation

and multi-UAV (unmanned aerial vehicle) deployment for business applications such as smart logistics warehousing, factory production lines, 3D scene scanning, or panoramic photography.

Throughout the evolution of cooperative perception, advancements in single-agent perception have consistently served as a significant reference point. For instance, fundamental computer vision backbones improve feature extraction capabilities, while attention mechanisms create correlations between features. In single-agent perception, there has been ongoing debate between the use of single-modality versus multi-modality approaches for commercial deployment of autonomous driving perception systems, balancing performance and cost. However, the current situation is that multi-modality offers clear advantages in most aspects of perception, such as accuracy, robustness, and detection range. This prevailing view is supported by the superior performance of multi-modality on various public datasets compared to single-modality approaches, since one more modality yield to richer representation features of object to be detected.

Meanwhile, in the realm of cooperative perception, existing methods have predominantly focused on fusing single unified modality data (e.g., LiDAR or camera) across multiple agents as depicted in Fig. 1 (b). It was not until the recent breakthroughs with HM-ViT [1] and HEAL [2] that certain forms of heterogeneous fusion became possible as depicted in Fig. 1 (c). However, both HM-ViT and HEAL still restrict themselves by sharing one modality of sensor data per agent only, meaning the full potential of multi-modality remains untapped and invalidated in multi-agent collaboration. Simply forcing fusion of multi-modality sensor data (e.g., LiDAR and camera) per agent on HM-ViT or HEAL could even lead to markedly degraded performance compared to LiDAR-only multi-agent setting, due to the poor depth estimation from the camera modality. Thus, the gap between multi-agent single-modality and full multi-agent multi-modality still exists. Moreover, alongside efforts to close this gap, maintaining fusion compatibility with single-modality agents is crucial, raising the question: *how can we fully leverage every possible sensor on every possible agent for cooperative perception?* While achieving high perception performance is the primary goal, we also recognize the importance of computational efficiency and communication support-ability for future industrial applications.

In this paper, we propose two novel multi-agent and multi-modality cooperative perception architectures: Paint-To-Puzzle (PTP) and Co-Sketching-Co-Coloring (CoS-CoCo),

*This work was supported by Sony (China) Limited

¹Lantao Li, Wenqi Zhang, Xiaoxue Wang and Chen Sun are with Sony Research and Development Center China, Beijing, China lantao.li@sony.com, wenqi.zhang@sony.com, xiaoxue.wang@sony.com, chen.sun@sony.com

²Kang Yang is with the School of Information, Renmin University of China, Beijing, China y1127238112@gmail.com

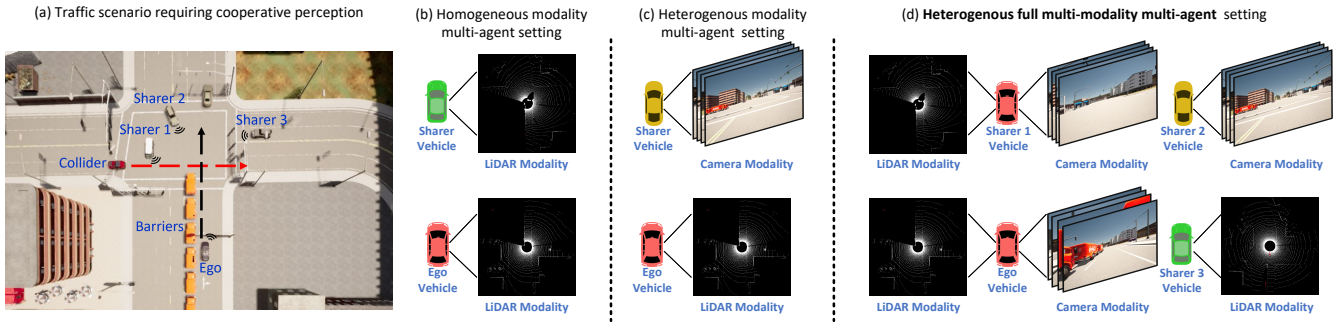


Fig. 1. (a) A typical traffic scenario where cooperative perception could be used to perceive through barriers and thus avoid collision. (b) Homogeneous modality multi-agent setting for conducting cooperative perception. (c) Heterogeneous modality multi-agent setting with a restriction on single modality per agent for conducting cooperative perception. (d) Heterogeneous full multi-modality multi-agent setting without restrictions on the number or types of modalities for conducting cooperative perception, partially covered by PTP and fully covered by CoS-CoCo.

each emphasizing different performance aspects based on the aforementioned motivations. PTP involves only one single inter-agent fusion step across all agents, with LiDAR modality as a mandatory requirement. This means that each participant performs its own cross-modality fusion before contributing to a unified fusion with all other agents. In contrast, CoS-CoCo uses a two-stage inter-agent fusion process: first fusion of LiDAR feature data among all agents equipped with LiDAR sensors, followed by fusion of camera feature data among all agents with camera sensors. Obviously, CoS-CoCo welcomes any agent with any sensor modality configuration to contribute. The choice between single-stage or two-stage cross-agent fusion affects the trade-off between PTP’s lower communication bandwidth requirements and CoS-CoCo’s broader diversity of sensor-sharing candidates, which leads to differences in perception performance. To enable efficient multi-modality fusion for both architectures, we design Radian-Glue-Attention (RG-Attn). RG-Attn samples the Bird’s Eye View (BEV) feature map constructed from LiDAR sensor data based on the divided radians of the camera’s field-of-view (FOV), enabling linear attention to each corresponding column of the camera feature map. This approach enhances the BEV feature map by incorporating the projected semantic information. Both PTP and CoS-CoCo outperform existing methods in the cooperative perception field by leveraging all available sensor sources as depicted in Fig. 1 (d), achieving dominant performance while significantly reducing training costs compared to most methods and maintaining real-time inference computational efficiency. In general, our contributions are as follows:

- We introduce RG-Attn, the first design to enable effective fusion of multi-modality data per agent for cooperative perception. RG-Attn is applicable to perform cross-modality fusion in both intra-agent and inter-agent scenarios, delivering robust and efficient performance.
- To unlock the potential of multi-modality in multi-agent cooperative perception, we propose PTP. To the best of our knowledge, PTP achieves SOTA performance on the mainstream cooperative perception datasets.
- We design CoS-CoCo as a prototype model with better

generalization ability for broader adaptability in practical heterogeneous deployment, validated in corresponding experiments on different combinations of modalities.

II. RELATED WORKS

A. Single-Agent Perception

In the realm of single-agent perception tasks, a proliferation of various single-modal approaches has made their debuts in the coliseum, successively contributing to the solid foundation for both single-modality and multi-modality approaches. Benchmarks like KITTI and nuScenes [21] have ignited competition in both LiDAR point cloud track and camera vision track. Point cloud data benefits greatly from backbones like PointNet [22], pillar encoding or voxel encoding, which facilitates feature aggregation to reconstruct concise and accurate representations. Meanwhile, camera vision track pioneers have progressed from monocular vision, and then achieved explosive performance growth through the multi-view data availability and the depth estimation concept brought by LSS [13]. Transformer structures, such as ViT and Point-Transformer [14], [15], have further elevated the performance of both single-modality tracks, ushering in a new era. Recently, LiDAR-track and camera-track have converged to the BEV-based algorithms [23], [24], enabling 3D object queries and position encoding for projection, location and aggregation, irrespective of modalities.

On the other hand, multi-modality approaches focus on the intrinsic relationships between LiDAR and camera data. This began with PointPainting [15] to add camera semantic information as an additional dimension to the LiDAR point cloud data, and delved into DETR-like structures [16] to exploit attention mechanisms for representation relationship discovery. BEV-based multi-modality fusion methods [9], [10] have emerged as a powerful platform for performing cross-modality mutual adaptation and attention, thanks to BEV’s ability to provide unified positional encoding and convenient query mechanisms for attention. Within the multi-modality domain, a recent trend [11], [12] has emerged that the relatively poor estimated depth from camera source should be abandoned for the cross-modality fusion. Instead,

they directly projected camera features via attention mechanisms onto the BEV space previously formed by point cloud data, thereby establishing a more robust cross-modality correspondence.

B. Multi-Agent Cooperative Perception

Multi-agent cooperative perception offers unique technical advantages by approaching perception problems from a more comprehensive perspective. With the increasing richness of cooperative perception datasets [7], [8], the field has seen the rise and fall of various technical approaches and research directions. Early techniques focused on early raw data fusion [19] for source data original richness and late fusion [20] of detection results for less communication overhead. More recent studies [1], [2], [3] have utilized the intermediate features for fusion to achieve the balance between model performance and V2X bandwidth requirements.

Within the cooperative perception framework, Who2Comm series [6], [30] focused on the priority of messages to transfer, FedBEVT [25] explored federated learning for cooperative perception, while Coopernaut and ICOP [4], [5] demonstrated how cooperative perception could enhance end-to-end (E2E) autonomous driving. For practical real-world deployment, studies such as CoAlign [26] and CBM [27] have demonstrated significant advancements in minimizing relative localization errors, a critical factor in the coordinate transformation across collaborative agents. Additionally, research from the vehicular wireless communication domain [28], [29], [30] has contributed to optimizing the communication protocol stack, aligning it with the upper-layer requirements of cooperative perception. The evolution of intermediate fusion methods has spanned concatenation-based, transformer-based, and pyramid-based approaches. Most existing works have focused on the single modality until recent HM-ViT [1] and HEAL [2] introduced multi-modality. However, both HM-ViT and HEAL limited their solution to only one modality of shared data per agent. The existing gap is how much can we improve if fully leverage all possible sensor sources efficiently to pursue an oracle-like vision, this critical issue is addressed in this paper.

III. METHODOLOGY

We first introduce the LiDAR and camera cross-modality fusion module as depicted in Fig. 2, and then expand on the design of two cooperative perception architectures that implement this fusion module as illustrated in Fig. 3 (a) and (b).

A. Radian-Glue-Attention (RG-Attn)

Since the generally inaccurate depth estimation from camera data is avoided, the key to successful cross-modality fusion lies in effectively projecting camera feature semantics onto the BEV feature space generated by the LiDAR backbone. Suppose the solid BEV feature map $F_j^{\text{bev}} \in \mathbb{R}^{C_1 \times H_1 \times W_1}$ and camera feature $F_{ik}^{\text{cam}} \in \mathbb{R}^{C_2 \times H_2 \times W_2}$ are generated from collaborative agents, where j and i denotes the sequence

number of agents and ik identify the camera k equipped on agent i . Since we do not limit the fusion to occur within a single system, the transformation matrix $T_{i \rightarrow j}$ of agent i to agent j considering the BEV grid size in reality world, along with the sensor k to its boarding agent transform $t_{ik \rightarrow i}$ are utilized for locating the camera sensor's location $t_{ik \rightarrow j}$ on the BEV feature map of agent j as $T_{i \rightarrow j} \cdot t_{ik \rightarrow i}$. The rotation part $R_{i \rightarrow j}$ out of transformation matrix $T_{i \rightarrow j}$ and the rotation matrix $R_{ik \rightarrow i}$ of camera k to its mounted agent i to form $R_{ik \rightarrow j}$ as $R_{i \rightarrow j} \cdot R_{ik \rightarrow i}$, will transfer the horizontal FOV angular interval $\left[-\frac{\theta_{\text{FOV}}}{2}, \frac{\theta_{\text{FOV}}}{2}\right]$ from camera k on agent i to agent j $\left[\theta_{ik \rightarrow j}^{\text{start}}, \theta_{ik \rightarrow j}^{\text{end}}\right]$ as $\left[\text{atan}\left(R_{ik \rightarrow j} \cdot u\left(-\frac{\theta_{\text{FOV}}}{2}\right)\right), \text{atan}\left(R_{ik \rightarrow j} \cdot u\left(\frac{\theta_{\text{FOV}}}{2}\right)\right)\right]$, where u stands for the angle unit vector.

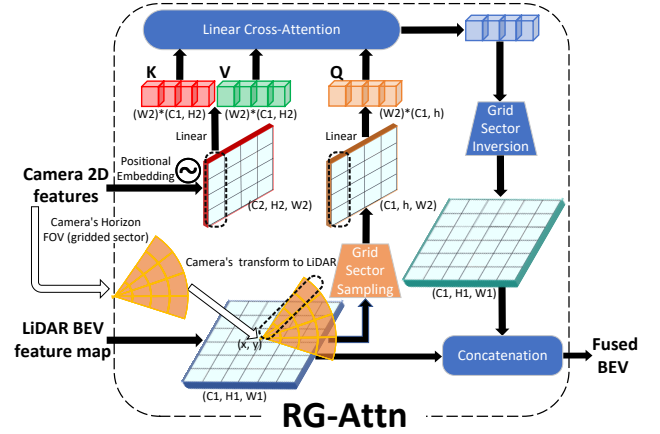


Fig. 2. RG-Attn structure enables cross-modality fusion between LiDAR BEV and camera 2D features. Camera sensor parameters (i.e., FOV, range, transform to LiDAR) configure the segmented grid sector for sampling the LiDAR BEV map to generate Queries. Camera features with learnable positional embedding provide Keys and Values. The BEV map's sampled width matches the camera feature width, allowing linear cross-modality multi-head attention. The fused features, after grid sector inversion, are concatenated with the original BEV map.

Once the relative transform and horizontal FOV range of camera k from agent i are determined on the target BEV map of agent j , a fundamental geometric relationship emerges. Specifically, the camera's horizontal FOV determines the angular span of its projected feature matrix on the BEV feature map. To establish the correspondence between the camera feature matrix and the BEV feature map, we segment the FOV into W_2 sub-sectors, each corresponding to a column in the camera feature matrix $F_{ik}^{\text{cam}} \in \mathbb{R}^{C_2 \times H_2 \times W_2}$. Each sub-sector is further divided along the radius into h grid segments, forming a gridded structure. The maximum fusion range R from camera semantics projection on the BEV feature map is defined based on the BEV grid granularity and is set to half of the BEV rectangle's diagonal length, balancing distortion and fusion range. The number of radial segments h to divide R , is set to H_1 in our setting. Bilinear sampling is employed to establish the correspondence between the sector grids and their overlapping regions on the BEV feature map.

This process involves constructing a circular gridded sector centered at $(t_{ik \rightarrow j})$, with an angular span $[\theta_{ik \rightarrow j}^{\text{start}}, \theta_{ik \rightarrow j}^{\text{end}}]$, angular resolution W_2 , radius length R and radial resolution h . The resulting sampling configuration set $\text{Set}_{ik \rightarrow j}$ is defined as: $(t_{ik \rightarrow j}, [\theta_{ik \rightarrow j}^{\text{start}}, \theta_{ik \rightarrow j}^{\text{end}}], W_2, R, h)$.

Thus, a grid sector sampling module is ready to extract a sector-shape sub-area of the original BEV and sample it into a rectangle-like feature space as $F_{ik \rightarrow j}^{\text{sub-bev}} \in \mathbb{R}^{C_1 \times H_1 \times W_2}$ as:

$$F_{ik \rightarrow j}^{\text{sub-bev}} = \text{GridSectorSample}(F_j^{\text{bev}}, \text{Set}_{ik \rightarrow j}). \quad (1a)$$

Cross-modality fusion is then carried out by implementing a multi-head attention mechanism, with the linear layer generating queries from $F_{ik \rightarrow j}^{\text{sub-bev}}$, and keys and values from F_{ik}^{cam} as:

$$\overline{F}_{ik \rightarrow j}^{\text{fus-bev}} = \text{Attn}(\text{LN}(F_{ik \rightarrow j}^{\text{sub-bev}}), \text{LN}(F_{ik}^{\text{cam}}), \text{LN}(F_{ik}^{\text{cam}})). \quad (1b)$$

The semantic information of camera feature matrix is “glued” onto the corresponding areas of the sampled BEV space based on the radians. Subsequently, grid sector inversion is applied to map the enhanced but distorted feature back to the original scale of the BEV feature map as:

$$F_{ik \rightarrow j}^{\text{fus-bev}} = \text{GridSectorInverse}(\overline{F}_{ik \rightarrow j}^{\text{fus-bev}}, \text{Set}_{ik \rightarrow j}). \quad (1c)$$

The inversion process utilizes the same geometric correspondence and reverses the sampling direction. Finally, the enhanced feature map $F_{ik \rightarrow j}^{\text{fus-bev}}$ and the original feature map F_j^{bev} are concatenated to output $F_{j+ik}^{\text{fus-bev}} \in \mathbb{R}^{C_1 \times H_1 \times W_1}$ as:

$$F_{j+ik}^{\text{fus-bev}} = \text{Cat}(F_j^{\text{bev}}, F_{ik \rightarrow j}^{\text{fus-bev}}). \quad (1d)$$

The overall process of RG-Attn, as described from equation (1a) to equation (1d), could be succinctly expressed by the following equation:

$$F_{j+ik}^{\text{fus-bev}} = \text{RG-Attn}(F_j^{\text{bev}}, F_{ik}^{\text{cam}}). \quad (1)$$

B. Paint-To-Puzzle (PTP)

The core concept in the design of PTP is that every agent strives to create the most accurate fused BEV feature map before engaging in cross-agent fusion. As depicted in Fig. 3 (a), agents equipped with both LiDAR and cameras “**paint**” individual perceived scenarios and then “**puzzle**” them together. Consequently, the RG-Attn cross-modality fusion module is applied only within single-agent system in PTP, creating $F_{ik \rightarrow i}^{\text{fus-bev}}$ multiple times, depending on the number n of cameras equipped on agent i . These semantically enriched features are then concatenated to form $F_{i+\sum_{k=1}^n ik}^{\text{fus-bev}}$ as:

$$F_{i+\sum_{k=1}^n ik}^{\text{fus-bev}} = \text{RG-Attn}(F_i^{\text{bev}}, \{F_{ik}^{\text{cam}} \mid k = 1, 2, \dots, n\}), \quad (2a)$$

where $i \in \text{AgentsSet}_{\text{LiDAR}+\text{camera}}$. For collaborative agents equipped with LiDAR only, the original BEV feature map is retained as input for the subsequent “puzzle” part.

The Pyramid Fusion module from HEAL [2] is adopted as the backbone for the “puzzle” part, fusing all BEV feature maps into a richer BEV space as:

$$F_{\text{PTP}} = f_{\text{pyramid fusion}}(F_{i+\sum_{k=1}^n ik}^{\text{fus-bev}}, F_m^{\text{bev}}), \quad (2b)$$

where $i \in \text{AgentsSet}_{\text{LiDAR}+\text{camera}}$ and $m \in \text{AgentsSet}_{\text{LiDAR}_{\text{only}}}$. The multi-scale fusion structure and foreground awareness enhance the fusion of semantically glued features or original LiDAR features from entirely different perspectives. This process excludes camera-only collaborative agents due to their lack of a solid and relatively accurate depth-rooted BEV map. Only one unified format of shared perception payload is required.

C. Co-Sketching-Co-Coloring (CoS-CoCo)

As depicted in Fig. 3 (b), CoS-CoCo could be clearly divided into two stages of fusion: **Co-Sketching**, which involves the fusion of LiDAR BEV feature maps among LiDAR-equipped agents to provide the basic skeleton of the perceived surrounding environment, and **Co-Coloring**, which projects camera features onto the skeleton formed in the first stage. Similar to the BEV feature map fusion in PTP, the Pyramid Fusion module is employed in the Co-Sketching stage to fuse all available BEV feature maps into a robust, unified BEV feature map $F_{\text{pyr}}^{\text{bev}} \in \mathbb{R}^{C_1 \times H_1 \times W_1}$ as:

$$F_{\text{pyr}}^{\text{bev}} = f_{\text{pyramid fusion}}(F_l^{\text{bev}}), \quad (3a)$$

where $l \in \text{AgentsSet}_{\text{LiDAR}}$, indicating that every collaborative agent equipped with LiDAR “co-sketches” the solid skeleton.

In the Co-Coloring stage, every feature matrix from all available camera sensor sources and corresponding encoders is subsequently “glued” onto the unified BEV feature map $F_{\text{pyr}}^{\text{bev}}$ by leveraging the robustness and flexibility of our RG-Attn cross-modality fusion module in heterogeneous agent settings. Depending on the total number of camera-equipped agents and the corresponding number of cameras onboard, the Co-Coloring process can be represented as:

$$F_{\text{CoS-CoCo}} = \text{RG-Attn}(F_{\text{pyr}}^{\text{bev}}, \{F_{ck}^{\text{cam}} \mid k = 1, 2, \dots, n\}), \quad (3b)$$

where $c \in \text{AgentsSet}_{\text{camera}}$ and n is the number of cameras per agent in the set. The key advantage of CoS-CoCo is that it re-integrates camera-only collaborative agents into the cooperative system, though it requires two different formats of cooperative perception payloads.

IV. EXPERIMENTS AND RESULTS

A. Datasets

To validate the effectiveness of our full multi-modality, multi-agent solution against previous approaches, we utilize the DAIR-V2X and OPV2V datasets for training and evaluation. Our primary focus is on DAIR-V2X during the derivation of the model design, as it is based on real-world cooperative perception data collected in Beijing Yizhuang Autonomous Driving Demonstration Zone, presenting practical challenges. The DAIR-V2X dataset contains 9K frames, each comprising raw data from a vehicle agent and a roadside unit (RSU) agent, with LiDAR and camera data available from both agents, though each agent is equipped with only one camera. Conversely, the CARLA-simulated OPV2V dataset provides over 11K frames across diverse scenarios, with each frame of scenario containing raw data

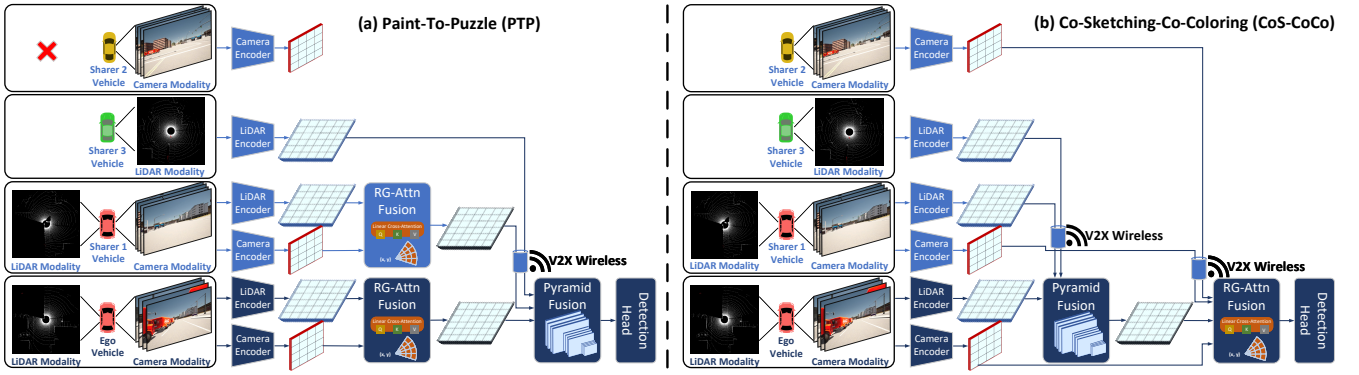


Fig. 3. In both the PTP and CoS-CoCo architectures, a single vehicle is designated as the ego vehicle to complete the full fusion process, while other vehicles perform preliminary steps before providing input to the ego vehicle. However, this process can also be fully and mutually carried out on each agent. (a) PTP requires only a single round of cross-agent fusion, as each participant contributes either a cross-modality fused BEV or a pure LiDAR-generated BEV. (b) CoS-CoCo incorporates all sensor sources from each participant, regardless of the sensor modality configuration (e.g., LiDAR-only, camera-only, or LiDAR-camera-both) in a two-stage cross-agent fusion process.

from 2 to 7 vehicles. Each vehicle in OPV2V is equipped with one LiDAR and four cameras in a unified manner.

In our experiments with both datasets, we consider three types of agents: LiDAR-only, camera-only, and LiDAR-camera-equipped. In OPV2V, all four cameras (800x600 resolution) are utilized for camera-equipped agents, with the default 64-channel 360° LiDAR for LiDAR-equipped agents, and no additional data enhancements are applied. For DAIR-V2X, both the RSU and vehicle provide 1920x1080 camera data, with notable variations in sensor placement heights. The RSU’s LiDAR has 300 channels with a 100° FOV, while the vehicle’s LiDAR is 40-channel with a 360° FOV.

B. Settings

Implementation details: We adopt unified encoders for raw data processing: PointPillar [18] for LiDAR point cloud and the first five sequential five layers of ResNet101 for camera images. The LiDAR BEV map is down-sampled 2x and further reduced to a shape of [64, 128, 256] using 3 consecutive ConvNeXt [17] blocks, with a grid size of [0.4m, 0.4m]. The feature matrix for each camera sensor after the encoder is in shape [8, 144, 256], as we fix the target channel, width and height of the output to deal with the different resolution specification in two datasets. In both PTP and CoS-CoCo, multi-head attention is configured with an embedding dimension of 64, attention heads of 8, and a dropout rate of 0.1. The pyramid fusion conducts multi-level fusion with widths (i.e., the last dimension of BEV map feature shape) at 256, 128 and 64 consequently. For fair comparison with existing SOTA approaches, the detection range in both training and evaluation is set to $x \in [-102.4m, +102.4m]$, $y \in [-51.2m, +51.2m]$. Object detection task head is added, and average precision (AP) is calculated at different intersection-over-union (IoU) thresholds.

Training configurations: Three loss function regarding the classification, regression and direction are used, incorporating foreground map output into loss calculation. We use Adam optimizer, with an initial learning rate set to

0.002 and decrease by 0.1 from epoch 15 to 25 for OPV2V and from epoch 35 to 40 for DAIR-V2X. On an NVIDIA RTX 6000 Ada, the training process with 30 epochs for OPV2V and 40 epochs for DAIR-V2X in total no matter the model is PTP or CoS-CoCo, costs approximately 6 hours for training on DAIR-V2X if setting batch size to 4. But for the OPV2V case, where the number of agents can reach up to 5 and each vehicle’s four-camera setup significantly increase computational demand, resulting in around 36 hours of training time due to GPU memory constraints.

C. Quantitative & Visualization Results

As shown in Table I, we compare the evaluation results of our approach with the best reported performances of existing methods [1], [2], [3], [8], [31], [32], [33] under identical conditions. Additionally, the performance results of the listed methods have been validated through our comparison experiments. To ensure a fair comparison, the number of collaborative agents is set to 2 (i.e., always two) for DAIR-V2X and 5 (i.e., maximum five) for OPV2V, with a fixed detection range. The key difference is that the compared methods achieve their peak performance using only LiDAR data from all collaborative agents, as reported in the corresponding papers. Notably, CoBEVT and HEAL exhibit performance degradation when incorporating camera data, as observed in the AP30 column of Table I and the LC+LC column under DAIR-V2X (AP30) of Table II (where both LiDAR and camera modalities are enabled for all agents without extending optimization). In contrast, our approach effectively leverages the complementary advantages of camera data. This improvement is particularly evident when comparing HEAL with our proposed methods, as our cross-modality fusion module is built upon LiDAR-only architecture of HEAL. Specifically, when restricted to LiDAR-only cross-agent fusion, both of our proposed models achieve the same performance as HEAL.

To assess the impact of the number of participating agents in cooperative perception on our proposed methods, we conduct a series of controlled experiments on the OPV2V

TABLE I

BEST PERFORMANCES OF EXISTING COOPERATIVE PERCEPTION APPROACHES AND OUR APPROACHES ON DIFFERENT DATASETS

Dataset	DAIR-V2X		OPV2V	
Method	AP30	AP50	AP50	AP70
F-Cooper	0.723	0.620	0.763	0.481
AttFusion	0.738	0.673	0.878	0.751
DiscoNet	0.746	0.685	0.882	0.737
V2XViT	0.785	0.521	0.917	0.790
CoBEVT	0.787	0.692	0.935	0.821
HM-ViT	0.818	0.761	0.950	0.873
HEAL	0.832	0.790	0.963	0.926
PTP (Ours)	0.862	0.817	0.970	0.945
CoS-CoCo (Ours)	0.854	0.811	0.965	0.937

TABLE II

THE PERFORMANCE COMPARISON REGARDING THE COMBINATION OF AGENTS NUMBER AND MODALITY SETTING IN DIFFERENT APPROACHES

Dataset	DAIR-V2X (AP30)				OPV2V (AP50)			
Modality	LC	LC+C	LC+L	LC+LC	LC	LC+C	LC+L	LC+LC
CoBEVT	0.146	0.553	0.589	0.588	0.472	0.604	0.647	0.643
HEAL	0.237	0.574	0.692	0.776	0.581	0.636	0.733	0.854
PTP	0.707	/	0.743	0.862	0.820	/	0.875	0.955
CoS-CoCo	0.705	0.712	0.848	0.854	0.821	0.837	0.944	0.949

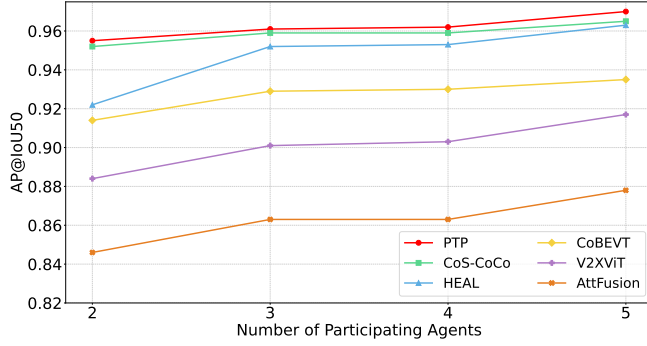


Fig. 4. AP50 performance of our methods and key baseline approaches under different maximum numbers of participating agents on OPV2V.

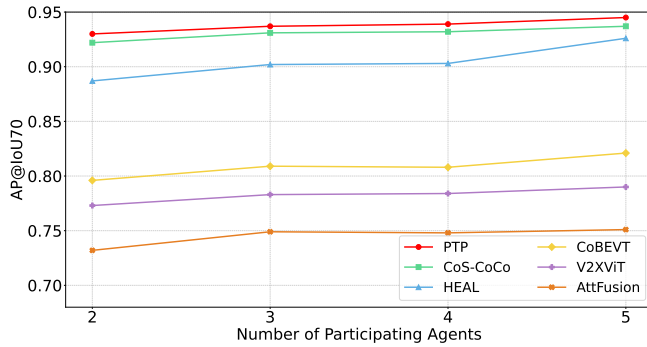
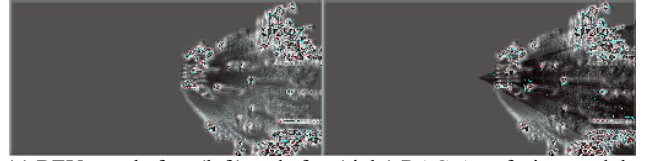


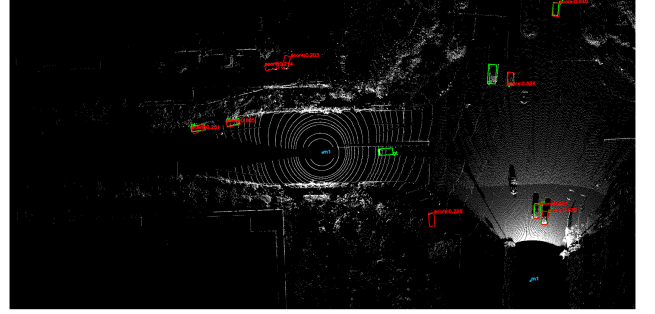
Fig. 5. AP70 performance of our methods and key baseline approaches under different maximum numbers of participating agents on OPV2V.

dataset. As illustrated in Fig. 4 and Fig. 5, these experiments systematically evaluate how performance scales with varying numbers of collaborating agents, providing insights into the effectiveness and adaptability of our approach under different cooperation levels.

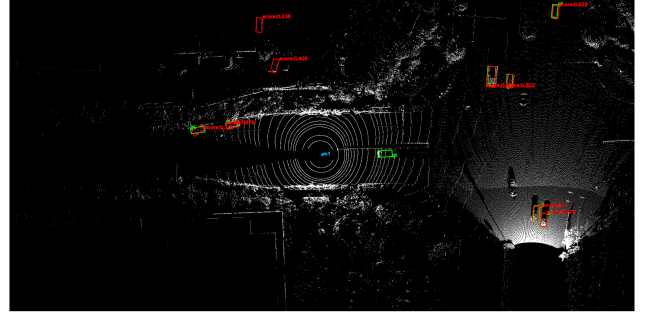
We further assess our methods' performances across var-



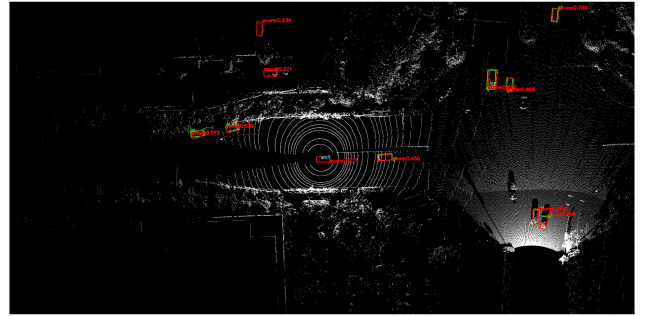
(a) BEV map before (left) and after (right) RAG-Attn fusion module



(b) HEAL (LiDAR-only multi-agent fusion)



(c) CoS-CoCo (LiDAR-camera-both multi-agent fusion)



(d) PTP (LiDAR-camera-both multi-agent fusion)

Fig. 6. The BEV map before RG-Attn and the cross-modality fused BEV map after RG-Attn is shown in (a), based on one frame of cross-modality data from DAIR-V2X RSU. Visualization of cooperative perception results comparing our methods against the previous SOTA method—HEAL are given from (b) to (d), the **ground truth** and the **predicted** bounding boxes are in corresponding colors.

ious combinations of agent numbers and modalities on both the DAIR-V2X dataset and the OPV2V dataset, as presented in Table II, where “+” separates two agents, “L” stands for LiDAR, “C” for camera, and “LC” for agent equipped with both LiDAR and camera. All models are trained only once with full multi-modality multi-agent setting (i.e., LC+LC), and directly used for all the inferences with different settings. The performances of HEAL and CoBEVT for conducting multi-modality, are achieved by their BEV fusion module to fuse all BEV feature maps from different modalities and

agents, decreased by 5.6% and 19.9% in DAIR-V2X AP30 compared to LiDAR-only case, reflecting their negatives of incorporating camera modality. A similar performance degradation could be also observed on OPV2V, with HEAL and CoBEVT experiencing declines of 6.8% and 27.1% in AP50, as reflected in Fig. 4 and the right half of Table II.

The corresponding communication budget for sharing the cooperative perception intermediate data is 4.56 Megabytes for PTP and 6.25 Megabytes for CoS-CoCo, representing one uncompressed data frame per agent. The inference time for PTP or CoS-CoCo is approximately 40 milliseconds when two collaborative agents are involved, with the RG-Attn module requiring no more than 4 milliseconds per fusion.

In addition to the quantitative results, visualizations of the intermediate cross-modality fusion via the RG-Attn module and the final object detection outcomes of our methods versus the previous SOTA method are shown in Fig. 6, respectively.

D. Performance Analysis

Fusion Effectiveness: Both PTP and CoS-CoCo surpass the existing methods, as shown in Table. I, largely due to the effective cross-modality fusion capabilities of the RG-Attn module. PTP achieves dominant performance on both datasets, surpassing the previous SOTA method HEAL by 3.0% in DAIR-V2X AP30 and 1.9% in OPV2V AP70, extracting the maximum potential from the current RG-Attn design. Such performance advantage of our proposed methods persists across varying numbers of participating agents, as shown in Fig. 4 and Fig. 5. This is attributed to the intra-agent fusion process, where camera semantic features are effectively “glued” to the intact sampled LiDAR-derived BEV feature map, fully transforming the camera features to enhance the BEV map. However, when conducting the cross-modality fusion in inter-agent stage of CoS-CoCo, the intersection area for sampling the BEV map to align with camera’s FOV might reach the boundary of LiDAR feature map or even no valid overlapping projection area, depending on the relative distance and direction of agents. Such cases can result in abnormal and fragmentary semantic information projection, leading to less effective fusion. The evident contrast can be observed in perception results visualization from Fig. 6 (b) to (d) consequently, with more objects identified and more accurate bounding boxes given incrementally.

Generalization: On the other hand, CoS-CoCo delivers more robustness and adaptability as shown in Table II, where performance does not fall off a cliff due to the heterogeneous modality settings. The CoS-CoCo model for evaluation does not require any additional training or re-training process to integrate agents with different modality configurations, reflecting its greater potential for real-world applications.

Ablation Component: The LiDAR-only cross-agent fusion setting for PTP or CoS-CoCo, representing the absence of RG-Attn for cross-modality fusion, leads to a performance degradation of 3.0% in AP30 and 2.7% in AP50 on DAIR-V2X, significantly higher than experimental error. Fig. 6 (a) can also reflect the essential functionality of RG-Attn, as

the output BEV feature map exhibits a more distinct feature distribution.

V. CONCLUSION AND FUTURE WORK

We view our work as an initial step toward achieving comprehensive multi-agent, multi-modality fusion in cooperative perception, with significant room for further performance improvements. The RG-Attn module could be refined to perform cross-modality fusion more accurately, and the overall framework could be expanded to integrate the strengths of both PTP and CoS-CoCo. In general, we have demonstrated the accuracy and efficiency of our novel designs for cooperative perception in this paper. We hope this work encourages further discussions and advancements in the field of multi-modality multi-agent cooperative perception.

REFERENCES

- [1] H. Xiang, R. Xu and J. Ma, “HM-ViT: Hetero-modal vehicle-to-vehicle cooperative perception with vision transformer,” in *2023 IEEE/CVF International Conference on Computer Vision (ICCV)*, Paris, France, 2023, pp. 284-295.
- [2] Y. Lu, Y. Hu, Y. Zhong, D. Wang, Y. Wang and S. Chen, “An Extensible Framework for Open Heterogeneous Collaborative Perception,” *arXiv preprint. arXiv:2401.13964*, 2024.
- [3] R. Xu, Z. Tu, H. Xiang, *et al.*, “CoBEVT: Cooperative bird’s eye view semantic segmentation with sparse transformers,” *arXiv preprint arXiv:2207.02202*, 2022.
- [4] J. Cui, H. Qiu, D. Chen, P. Stone and Y. Zhu, “Coopernaut: End-to-End Driving with Cooperative Perception for Networked Vehicles,” in *2022 IEEE/CVF Conference on Computer Vision and Pattern Recognition (CVPR)*, New Orleans, LA, USA, 2022, pp. 17231-17241.
- [5] L. Li, Y. Cheng, C. Sun and W. Zhang, “ICOP: Image-based Cooperative Perception for End-to-End Autonomous Driving,” in *2024 IEEE Intelligent Vehicles Symposium (IV)*, Jeju Island, Korea, Republic of, 2024, pp. 2367-2374.
- [6] Y.C. Liu, J. Tian, C.Y. Ma, N. Glaser, C.W. Kuo and Z. Kira, “Who2com: Collaborative Perception via Learnable Handshake Communication,” in *2020 IEEE International Conference on Robotics and Automation (ICRA)*, Paris, France, 2020, pp. 6876-6883.
- [7] H. Yu *et al.*, “DAIR-V2X: A Large-Scale Dataset for Vehicle-Infrastructure Cooperative 3D Object Detection,” in *2022 IEEE/CVF Conference on Computer Vision and Pattern Recognition (CVPR)*, New Orleans, LA, USA, 2022, pp. 21329-21338.
- [8] R. Xu, H. Xiang, X. Xia, X. Han, J. Li and J. Ma, “OPV2V: An Open Benchmark Dataset and Fusion Pipeline for Perception with Vehicle-to-Vehicle Communication,” in *2022 International Conference on Robotics and Automation (ICRA)*, Philadelphia, PA, USA, 2022, pp. 2583-2589.
- [9] Z. Liu *et al.*, “BEVFusion: Multi-Task Multi-Sensor Fusion with Unified Bird’s-Eye View Representation,” in *2023 IEEE International Conference on Robotics and Automation (ICRA)*, London, United Kingdom, 2023, pp. 2774-2781.
- [10] C. Yang *et al.*, “BEVFormer v2: Adapting Modern Image Backbones to Bird’s-Eye-View Recognition via Perspective Supervision,” in *2023 IEEE/CVF Conference on Computer Vision and Pattern Recognition (CVPR)*, Vancouver, BC, Canada, 2023, pp. 17830-17839.
- [11] H. Zhang, *et al.*, “SparseLIF: High-Performance Sparse LiDAR-Camera Fusion for 3D Object Detection,” *arXiv preprint. arXiv:2403.07284*, 2024.
- [12] J. Gunn, *et al.*, “Lift-Attend-Splat: Bird’s-eye-view camera-lidar fusion using transformers,” in *Proceedings of the IEEE/CVF Conference on Computer Vision and Pattern Recognition (CVPR) Workshops*, Seattle, WA, USA, 2024, pp. 4526-4536.
- [13] J. Philion and S. Fidler, “Lift, splat, shoot: Encoding images from arbitrary camera rigs by implicitly unprojecting to 3D,” in *2020 European Conference on Computer Vision (ECCV)*, 2020, pp. 194-210.
- [14] H. Zhao, L. Jiang, J. Jia, P. Torr and V. Koltun, “Point Transformer,” in *2021 IEEE/CVF International Conference on Computer Vision (ICCV)*, Montreal, QC, Canada, 2021, pp. 16239-16248.

- [15] S. Vora, A. H. Lang, B. Helou and O. Beijbom, "PointPainting: Sequential Fusion for 3D Object Detection," in *2020 IEEE/CVF Conference on Computer Vision and Pattern Recognition (CVPR)*, Seattle, WA, USA, 2020, pp. 4603-4611.
- [16] Y. Wang, *et al.*, "Detr3d: 3d object detection from multi-view images via 3d-to-2d queries," in *2022 Conference on Robot Learning PMLR*, pp. 180-191.
- [17] Z. Liu, H. Mao, C. -Y. Wu, C. Feichtenhofer, T. Darrell and S. Xie, "A ConvNet for the 2020s," in *2022 IEEE/CVF Conference on Computer Vision and Pattern Recognition (CVPR)*, New Orleans, LA, USA, 2022, pp. 11966-11976.
- [18] A. H. Lang, S. Vora, H. Caesar, L. Zhou, J. Yang and O. Beijbom, "PointPillars: Fast Encoders for Object Detection From Point Clouds," in *2019 IEEE/CVF Conference on Computer Vision and Pattern Recognition (CVPR)*, Long Beach, CA, USA, 2019, pp. 12689-12697.
- [19] Q. Chen, S. Tang, Q. Yang and S. Fu, "Cooper: Cooperative Perception for Connected Autonomous Vehicles Based on 3D Point Clouds," in *2019 IEEE 39th International Conference on Distributed Computing Systems (ICDCS)*, Dallas, TX, USA, 2019, pp. 514-524.
- [20] Z. Y. Rawashdeh and Z. Wang, "Collaborative Automated Driving: A Machine Learning-based Method to Enhance the Accuracy of Shared Information," in *2018 21st International Conference on Intelligent Transportation Systems (ITSC)*, Maui, HI, USA, 2018, pp. 3961-3966.
- [21] H. Caesar *et al.*, "nuScenes: A Multimodal Dataset for Autonomous Driving," in *2020 IEEE/CVF Conference on Computer Vision and Pattern Recognition (CVPR)*, Seattle, WA, USA, 2020, pp. 11618-11628.
- [22] R. Q. Charles, H. Su, M. Kaichun and L. J. Guibas, "PointNet: Deep Learning on Point Sets for 3D Classification and Segmentation," in *2017 IEEE Conference on Computer Vision and Pattern Recognition (CVPR)*, Honolulu, HI, USA, 2017, pp. 77-85.
- [23] Y. Chen *et al.*, "FocalFormer3D : Focusing on Hard Instance for 3D Object Detection," in *2023 IEEE/CVF International Conference on Computer Vision (ICCV)*, Paris, France, 2023, pp. 8360-8371.
- [24] Z. Zong *et al.*, "Temporal Enhanced Training of Multi-view 3D Object Detector via Historical Object Prediction," in *2023 IEEE/CVF International Conference on Computer Vision (ICCV)*, Paris, France, 2023, pp. 3758-3767.
- [25] R. Song, R. Xu, A. Festag, J. Ma and A. Knoll, "FedBEVT: Federated Learning Bird's Eye View Perception Transformer in Road Traffic Systems," *IEEE Transactions on Intelligent Vehicles*, vol. 9, no. 1, pp. 958-969.
- [26] Y. Lu *et al.*, "Robust Collaborative 3D Object Detection in Presence of Pose Errors," in *2023 IEEE International Conference on Robotics and Automation (ICRA)*, London, United Kingdom, 2023, pp. 4812-4818.
- [27] Z. Song, T. Xie, H. Zhang, J. Liu, F. Wen and J. Li, "A Spatial Calibration Method for Robust Cooperative Perception," *IEEE Robotics and Automation Letters*, vol. 9, no. 5, pp. 4011-4018, May 2024.
- [28] L. Li, W. Zhang, X. Wang, T. Cui and C. Sun, "NLOS Dies Twice: Challenges and Solutions of V2X for Cooperative Perception," *IEEE Open Journal of Intelligent Transportation Systems*, vol. 5, pp. 774-782, 2024.
- [29] Y. Asabe, E. Javanmardi, J. Nakazato, M. Tsukada and H. Esaki, "AutowareV2X: Reliable V2X Communication and Collective Perception for Autonomous Driving," in *2023 IEEE 97th Vehicular Technology Conference (VTC2023-Spring)*, Florence, Italy, 2023, pp. 1-7.
- [30] Y. Hu *et al.*, "Where2comm: Communication-Efficient Collaborative Perception via Spatial Confidence Maps," *Advances in Neural Information Processing Systems*, vol. 35, pp. 4874-4886.
- [31] Q. Chen, X. Ma, S. Tang, J. Guo, Q. Yang and S. Fu, "F-cooper: Feature based cooperative perception for autonomous vehicle edge computing system using 3D point clouds," in *Proceedings of the 4th ACM/IEEE Symposium on Edge Computing*, 2019, pp. 88-100.
- [32] E. Mehr, A. Jourdan, N. Thome, M. Cord and V. Guitteny, "DiscoNet: Shapes Learning on Disconnected Manifolds for 3D Editing," in *2019 IEEE/CVF International Conference on Computer Vision (ICCV)*, Seoul, Korea (South), 2019, pp. 3473-3482.
- [33] R. Xu, H. Xiang, Z. Tu, X. Xia, M.H. Yang and J. Ma, "V2x-vit: Vehicle-to-everything cooperative perception with vision transformer," in *2022 European Conference on Computer Vision (ECCV)*, 2022, pp. 107-124.